

We are IntechOpen, the world's leading publisher of Open Access books Built by scientists, for scientists

6,900

Open access books available

186,000

International authors and editors

200M

Downloads

Our authors are among the

154

Countries delivered to

TOP 1%

most cited scientists

12.2%

Contributors from top 500 universities



WEB OF SCIENCE™

Selection of our books indexed in the Book Citation Index
in Web of Science™ Core Collection (BKCI)

Interested in publishing with us?
Contact book.department@intechopen.com

Numbers displayed above are based on latest data collected.
For more information visit www.intechopen.com



Median Effect Dose and Combination Index Analysis of Cytotoxic Drugs Using Flow Cytometry

Tomás Lombardo, Laura Anaya, Laura Kornblihtt and Guillermo Blanco
*Laboratory of Immunotoxicology (LaITo), Hospital de Clínicas San Martín,
University of Buenos Aires
Argentina*

1. Introduction

Targeted therapy is a strategy of anticancer treatment that aims to interfere with processes of tumorigenesis, cancer progression and metastasis by selectively affecting key molecules of tumor cells (Armand et al., 2007; Favoni & Florio, 2011; Gross-Goupil & Escudier, 2010). Targeted therapies are directed to small molecules participating in different mechanisms that control cell survival through cellular proteins or signalling pathways (Mueller et al., 2009; Zahorowska et al., 2009). Targeted therapies may offer enhanced efficacy, enhanced selectivity, and less toxicity. However, targeting selective molecules and pathways often induces the activation of redundant mechanisms and enhances the emergence of resistant cells due to selective pressure (Woodcock et al., 2011). This is one of the reasons why the effects of targeted agents are not durable when used alone, and often result in drug resistance and clinical relapse.

Except for specific cases the use of these targeted drugs as monotherapy is often discouraged due to lack of efficacy. However, combined therapy with drugs targeting several mechanisms of tumor cell death can greatly improve efficacy and may overcome resistance. Several genomic and epigenetic alterations have been identified in tumor cells that lead to unrestrained proliferation, evasion of proapoptotic signals, metastasis, and resistance to drug-induced cell death. These alterations are critical for cancer progression and therefore combination strategies employing multiple targeted agents can be a successful therapeutic strategy. In vertical combination strategies two or more drugs target a same pathway at two different points, while in horizontal combinations drugs are directed towards different intracellular signalling pathways and have the potential advantage of combining agents with non-overlapping toxicities (Gross-Goupil & Escudier, 2010).

Novel treatments require the investigation of mechanisms of action and synergy of combination treatments to enhance the role of the targeted pharmacological agents (Carew et al., 2008; Mitsiades et al., 2011). Evaluating combinations of targeted drugs, including investigational agents, are an essential part of this effort (Dancey & Chen, 2006). An interesting example is represented by Bortezomib, a drug currently effective as single agent in multiple myeloma and mantle cell lymphoma (Bross et al., 2004; Kane et al., 2007; Wright,

2010). Bortezomib is a proteasome inhibitor that selectively triggers apoptosis in various types of neoplastic cells. It has been tested in a wide variety of solid tumors but has generally been ineffective as monotherapy (Boccardo et al., 2005). However Bortezomib has shown increased activity when combined with several novel targeted agents including protein deacetylase inhibitors, kinase inhibitors, farnesyltransferase inhibitors, HSP-90 inhibitors, pan-Bcl-2 family inhibitors, and other classes of targeted inhibitors (Dai et al., 2003; Karp & Lancet, 2005; Pei et al., 2004; Perez-Galan et al., 2008; Trudel et al., 2007; Workman et al., 2007; Yanamandra et al., 2006). Thus, Bortezomib in combination with novel targeted therapies increase antitumor activity and overcome specific cellular antiapoptotic mechanisms (Wright, 2010).

Two-drug combination therapies are being assessed in a variety of tumors, usually testing agents that have different targets, nonoverlapping toxicity, and some rationale for evaluation (Belinsky et al., 2011; Castaneda & Gomez, 2009; Eriksen et al., 2009; Klosowska-Wardegga et al., 2010). An increase in the number of these studies is expected in coming years, on the basis of emerging data with new agents, which is expanding our understanding of the molecular pathways important in cancer progression. (Woodcock et al., 2011). Tumor intracellular signalling pathway dependencies are being increasingly analyzed, and patients treated on the basis of resistance profile detected for specific drug combinations (Busch et al.; Derenzini et al., 2009; Michiels et al., 2011). This approach may facilitate the development of combination regimens optimized for specific tumor subtypes, thus providing the potential for tailored therapy in individual patients on the basis of certain molecular and genetic characteristics of their disease.

1.1 Targeted drugs often induce programmed cell death as their main mechanism of anti-tumor activity

Many of the classic chemotherapeutic agents (alkylating agents, antimetabolites, antibiotics, topoisomerase inhibitors) are known to block cell division by compromising DNA replication and halting cell cycle progression, or inhibit mitosis, eventually leading to cell death (Foye, 1995; Goodman et al., 2010; Shuck & Turchi, 2010). Indicators of cell proliferation are suitable effect biomarkers to assess whether a combination of these agents is synergic, additive or antagonistic. Biomarkers frequently used for this purpose include incorporation of nucleotide analogues such as bromodeoxyuridine, or metabolic indicators of cell number such as tetrazolium salt-based assays (Karaca et al., 2009; Olszewska-Slonina et al., 2004; Sims & Plattner, 2009). However many of the new targeted agents interfere with constitutively active survival pathways or initiate apoptosis by directly influencing pro-apoptotic signals (Citri et al., 2004; Kim et al., 2005; Larsen et al., 2011; Vega et al., 2009; Zhang et al., 2009). In addition autophagic cell death and programmed necrosis are being actively investigated as alternative and pharmacologically relevant forms of programmed cell death (Berghe et al., 2010; Bijnsdorp et al., 2011; Duan et al., 2010; Gozuacik & Kimchi, 2007; McCall, 2010; Notte et al., 2011; Paglin et al., 2005; Platini et al., 2010). Combination studies should be conducted using effect biomarkers that are as close as possible to the known mechanisms targeted by single agents, and biomarkers specifically related to drug-induced tumor cell death appear more adequate for the assessment of new targeted agents (Cameron et al., 2001; Facoetti et al., 2008; Wesierska-Gadek et al., 2005). A straightforward approach is to determine the proportion of live and dead cells in viability studies scoring

thousands of cells through flow cytometry which ensures exceptional precision for dose-effect cytotoxicity studies.

2. Assessment of viability through flow cytometry

The strength of flow cytometry when compared to other methods available to assess the proportion of live and dead cells is the accuracy and precision brought by single cell multiparametric assessment. A variety of fluorescent probes may be chosen to use in viability assessment through flow cytometry. These probes are based on cell functions and biological conditions that are differentially preserved in live cells and lost in dead cells. It is usual to select at least two probes measuring independent functional conditions. For example, a probe evaluating membrane integrity of cells and another probe evaluating enzymatic activity. Probes should be selected to match specific experimental requirements such as biological variability, duration of the experiments, whether cells exposed to drugs are adherent or non-adherent, and illumination lines available in the flow cytometer. Some probes may be released after being retained within the cells for a short time and require immediate assessment through the flow cytometer after labelling, while others may be retained for several hours or may be even retained indefinitely by being covalently linked to cellular components. In addition some specimens may require fixation due to biohazard issues, so another kind of probes should be chosen and combined in these cases (De Clerck et al., 1994).

2.1 Fluorescent staining of live and dead cells

Viability is not easily defined in terms of a single physiological or morphological parameter. No single parameter fully defines cell death in all systems; therefore, it is often advantageous to use more than one cell death indicators based on different parameters such as membrane damage, and enzymatic or metabolic activity. A considerably large number of fluorescent probes have been introduced in the recent years that are dedicated to the assessment of viability on a single cell basis. Many of these new probes have features that are useful under specific experimental circumstances. The two conditions most often detected are increased cell membrane permeability in dead cells and the presence of enzymatic activity in live cells. The former is assessed with probes that become fluorescent when bound to DNA but are not able to pass through cell membrane if selective permeability is preserved, while the later is determined by fluorogenic substrates. However other conditions occurring only in live cells may be used to demonstrate viability such as enzymatic oxidation, reduction and mitochondrial membrane potential (Callewaert et al., 1991). It is important to underscore this concept because these probes are often used for assessment of specific cellular functions and it may be erroneously assumed that they have no contribution to the assessment of viability.

2.2 Enzymatic activity in live cells, use of tracker dyes

One of the first probes introduced and most frequently used to stain live cells has been fluorescein-diacetate (FDA) (Jones & Senft, 1985; Ross et al., 1989). This non-fluorescent cell-permeant esterase substrate penetrates the cell and is converted by nonspecific intracellular esterases into fluorescein.

Thus it becomes a more polar compound and is retained within those cells that have intact plasma membranes. In contrast, nonfluorescent FDA and fluorescein rapidly leak from those cells that have a damaged cell membrane because it is no longer retained due to increased permeability (Prosperi et al., 1986). This property ensures that dead cells will never retain FDA or fluorescein, even if cell death occurs after the labelling procedure. This is one of the reasons why it is recommended to analyze cells rapidly through the flow cytometer after staining with FDA and why they should be kept in low incubation temperatures to minimize potential fluorescein leakage.

Calcein-acetoxymethyl-ester (Calcein-AM) is a derivative of calcein that has several improvements over FDA (Duan et al., 2010; Papadopoulos et al., 1994). Calcein-AM is also a substrate of nonspecific intracellular esterases. The fluorescent product is calcein and is better retained in cells because it is a polyanionic compound that has six negative charges and two positive charges at pH 7. Calcein-Blue-AM and Calcein-Violet-AM are similar to Calcein-AM but have different excitation and emission wavelengths (Fuchs et al., 2007). Calcein-Blue-AM is excited with UV lasers while Calcein-Violet-AM is excited with 405 nm violet diode lasers, although both dyes emit blue fluorescence (Prowse et al., 2009). They can be used when the green fluorescence channel from the 488 nm excitation line is needed for other purpose and a UV or violet illumination line is available. Chloromethyl-fluorescein-diactate (CM-FDA), is a FDA derivative that is retained within the cell even after damage to the plasma membrane due to its ability to bind thiol groups (Lantz et al., 2001; Sarkar et al., 2009). The weakly thiol-reactive chloromethyl moieties of this compound react with intracellular thiols and the acetate groups are cleaved by cytoplasmic esterases (West et al., 2001). This compound will not stain dead cells but the label will be preserved in those cells that die after the labelling procedure because the fluorescent product will be bound to SH groups within the cells (Sebastia et al., 2003). Chloromethyl SNARF-1 acetate is similar to CM-FDA but exhibits red fluorescence when excited with 488 nm blue laser. Thus it can be used when the green fluorescence channel is needed for other purpose and a UV or violet illumination line is not available (Hamilton et al., 2007). Carboxy-fluorescein-succinimidyl-ester (CFSE) is converted to fluorescent compound by intracellular esterases but covalently

Probe	Excitation line	Fluorescence emission	Intracellular retention
FDA	Blue	Green	Poor
Calcein-AM	Blue	Green	Good
Calcein Blue-AM	UV	Blue	Good
Calcein Violet-AM	Violet	Blue	Good
5-CI-M-FDA	Blue	Green	Excellent
5-CI-M-SNARF	Blue	Orange	Excellent
CFSE	Blue	Green	Excellent

Table 1. Fluorogenic substrates of intracellular esterases that are commonly used as viability probes

binds amino groups of proteins and is completely retained within cells, even after damage of cell membrane (Fujioka et al., 1994; Li et al., 2003). This dye is also used as cell tracker because it is retained in daughter cells after several rounds of cell division (Parish & Warren, 2002). It is worth to note that probes like FDA may give poor results with trypsinized cells owing to potential leakage of fluorescein during the staining and washing procedures (Zamai et al., 2001). Thus probes like CM-FDA, CM-SNARF-1, and CFSE may be a better choice for staining adherent cells.

2.3 DNA labelling in live and dead cells

Many polar nucleic acid stains are able to enter eukaryotic cells only when the plasma membrane is damaged. These stains are known as cell-impermeant dyes and include propidium iodide (PI) which is the most frequently used probe for assessing viability in flow cytometry (Yeh et al., 1981). This dye is excluded from live cells because it is negatively charged but readily penetrates the membrane of damaged cells and binds DNA. When excited at 488 nm DNA-bound PI increases orange-red fluorescence emission more than 1000 fold. Another commonly used cell-impermeant dye excited with 488 nm laser is 7-aminoactinomycin-D (7AAD). This dye binds DNA only in dead cells but emits fluorescence beyond 610 nm and allows the usage of the yellow-orange fluorescence channel for other purpose (Pallis et al., 1999).

Both PI and 7AAD have large Stokes shifts and can be used in 488 nm laser flow cytometers with green fluorescent tracker dyes such as FDA, CM-FDA, Calcein-AM and CFSE. Cells with damaged membranes may be identified with other cell-impermeant DNA fluorescent dyes that emit fluorescence in different wavelengths than that of PI.

The SYTOX series includes SYTOX-green (excited with 488 nm laser), SYTOX-red (excited with 633 and 635 nm lasers) and SYTOX-blue (excited with UV or 405 nm violet diode laser) (Haase, 2004; Lebaron et al., 1998; Yan et al., 2005). In contrast to SYTOX dyes, the SYTO series of nucleic acid stains can enter live cells and are thus cell-permeant DNA dyes (Ullal et al., 2010). The SYTO probes bind DNA with low affinity in live or dead cells (Eray et al., 2001; Poot et al., 1997). They are combined with high affinity cell-impermeant dyes to discriminate live from dead cells (Wlodkowic & Skommer, 2007). For example cell-permeant SYTO-red will stain live and dead cells with red fluorescence binding with low affinity to DNA, but if used together with SYTOX-green dead cells will be green fluorescent, because SYTOX-green has much higher affinity for DNA and will displace the low affinity SYTO-red. In addition, SYTOX-green will never stain live cells because it is cell-impermeant.

2.4 Biohazardous specimens

Viability staining of biohazardous specimens often requires fixation procedures that inactivate pathogens but produce minimal distortion of cellular characteristics. Some combinations of cell permeant and cell impermeant DNA dyes can be treated with fixatives such as 4% glutaraldehyde or formaldehyde to allow safer handling during analysis, without disrupting the distinctive staining pattern. An example is provided by cell-permeant, green-fluorescent DNA probe SYTO-10 and the cell-impermeant, red-fluorescent DNA probe ethidium homodimer-2 (Barnett et al., 2004; Poole et al., 1996). Using these two probes cells can be stained and fixed at various times during an experiment, and the results

can be analyzed several hours later. This method may be applied to viability assessment of any non-adherent cells, as well as trypsinized adherent cells. Tables 1, 2, and 4 summarize the main features of viability probes based on enzymatic activity and DNA labelling discussed above that may be considered to meet specific experimental requirements.

Probe	Excitation line	Fluorescence emission	Membrane Permeant	DNA Affinity	Fixable
SYTOX-Blue	UV-Violet	Blue	NO	High	NO
SYTOX-Green	Blue	Green	NO	High	NO
SYTOX-Red	Red	Red	NO	High	NO
Propidium iodide	Blue	Orange-Red	NO	High	NO
7AAD	Blue	Red	NO	High	NO
SYTO-10	Blue	Green	YES	Low	YES
SYTO-Red	Blue	Red	YES	Low	NO
Ethidium homodimer-2	Blue	Green	NO	High	YES

Table 2. DNA probes used for viability assessment

2.5 Two parameter assessment of viability through flow cytometry

Identification of live and dead cells is often conducted with simultaneous use of two probes. The combination may include a cell-impermeant DNA probe and either a fluorogenic substrate or a cell-permeant DNA probe. It should be highlighted that viability may be also indicated by probes that have been designed to assess other cellular functions. For example generation of hydrogen peroxide and superoxide anion occurs in live cells due to normal function of mitochondrial electron transport chain and does not occur in dead cells. The superoxide anion probe dihydroethidine (HE) and the hydrogen-peroxide probe dihydro-dichloro-fluoresceindiacetate (DH-DCFDA) will stain live cells red fluorescent and green fluorescent respectively (Eruslanov & Kusmartsev, 2010; Zanetti et al., 2005). Both probes may be appropriately combined with cell-impermeant DNA dyes to discriminate between live and dead cells.

Similarly potentiometric dyes stain live cells with preserved mitochondrial membrane potential, but not dead or compromised live cells where the mitochondrial membrane potential has collapsed (Marchetti et al., 2004). Thus they may also be combined with cell-impermeant DNA dyes to discriminate live and dead cells. For example, rhodamine 123 has been used in combination with propidium iodide for viability assessment with two-color flow cytometry (Darzynkiewicz et al., 1982). Metabolically active cells undergo normal oxidation-reduction reactions and thus can also reduce a variety of probes, providing a measure of cell viability and overall cell health (Callewaert et al., 1991; Radcliff et al., 1991). Resazurin and dodecylresazurin (C12-resazurin) have been extensively used as oxidation-reduction indicators to detect viable cells (Czekanska, 2011). Reduction of resazurin yields

the red fluorescent product resorufin while C12-resazurin yields C12-resorufin which is better retained by single cells (Talbot et al., 2008).

Again these probes may be combined with cell-impermeant DNA probes like SYTOX-green to discriminate live and dead cells with two color flow cytometry.

2.6 Viability assessment with single-color fixable dyes

In some experimental circumstances only one fluorescence channel may be dedicated to assessment of cell viability. In this case amine-reactive fluorescent dyes can be used to evaluate mammalian cell viability.

In cells with compromised membranes, these dyes react with free amines both in the cell interior and on the cell surface, yielding intense fluorescent staining. In viable cells, the dyes only stain cell-surface amines, resulting in less intense fluorescence (Elrefaei et al., 2008). The difference in intensity between the live and dead cell populations is preserved following formaldehyde fixation, using conditions that inactivate pathogens (Burmeister et al., 2008). There are several options of fluorescence excitation (UV, violet, blue, and red lasers) and emission wavelength (blue, green, yellow, red).

Probe	Excitation line	Fluorescence emission
LIVE/DEAD® fixable Blue	UV	Blue-450 nm
LIVE/DEAD® Fixable Aqua	UV	Green-526 nm
LIVE/DEAD® Fixable Yellow	Violet	Yellow-575 nm
LIVE/DEAD® Fixable Violet	Violet	Blue-450 nm
eFluor® 450	Violet	Blue-450 nm
Fixable Viability Stain 450®	Violet	Blue-450 nm
LIVE/DEAD® Fixable Green	Blue	Green-520 nm
eFluor® 506	Blue	Green-506 nm
LIVE/DEAD® Fixable Red	Red	Red-615 nm
LIVE/DEAD® Fixable Far Red	Red	Far Red-665 nm
eFluor® 660	Red	Far Red-660 nm

Table 3. Fixable amine-reactive fluorescent probes used for single-color assessment of cell viability. The wavelengths indicated correspond to the emission peaks as specified by the probe manufacturer

2.7 Viability vs. apoptosis

Most targeted cytotoxic drugs have been shown to induce apoptosis or other modes of programmed cell death, including autophagic cell death or programmed necrosis. These mechanisms of cell death are often contrasted to necrosis where a passive, sudden and uncontrolled disintegration of the cell occurs. Physiological consequences of apoptosis and passive necrosis are different, and thus it is important to determine the cell death phenotype. When assessed through flow cytometry, cells undergoing apoptosis or other forms of programmed cell death show a decrease in cell volume and forward light scatter (FSC), and an increase in side light scatter (SSC) mainly due to cytoplasmic and nuclear changes such as blebbing, and nuclear fragmentations (Dive et al., 1992; Pheng et al., 2000). In contrast necrosis often shows increased cell volume and FSC without changes in SSC (Healy et al., 1998). Viability assessment after cytotoxic drug exposure does not address the cell death phenotype, thus any kind of cell death phenotype may be induced by drug treatment including passive necrosis (Healy et al., 1998). However studies determining the median cytotoxic dose will require exposure to increasing doses from sub-lethal levels to the minimal doses approaching 100% cell death. In this scenario, programmed cell death phenotypes are more frequently observed than passive necrosis.

Probe	Membrane Permeant	Excitation line	Fluorescence emission
YOYO-1	NO	Blue	Green
TOTO	NO	Blue	Green
TO-PRO	NO	Blue	Green
POPO-1	NO	UV-Violet	Blue
BOBO-1	NO	UV-Violet	Blue
YOYO-3	NO	Red	Red
TOTO-3	NO	Red	Far Red
BOBO-3	NO	Red	Red
JOJO-1	NO	Green	Orange
JO-PRO-1	NO	Green	Orange

Table 4. Membrane-impermeant dimeric and monomeric cyanine dyes are nonfluorescent unless bound to nucleic acids and have extinction coefficients 10–20 times greater than that of DNA-bound propidium iodide

2.8 FDA-PI staining and the "cell death pathway": Frequency distributions of graded and abrupt transitions

When two fluorescent probes are used to determine the proportion of live and dead cells after exposure to cytotoxic drugs over an extended dose range data analysis would be better analyzed on a bivariate plot.

An example is the pair represented by FDA as an indicator of esterase activity in live cells and PI as an indicator of cell membrane damage (Fig. 1). In this case a bivariate plot of green fluorescence against red fluorescence will aid in determining the percentage of live and dead cells (Fig. 1A,C). In addition, the bivariate plot will provide useful data about the biological processes evaluated with FDA and PI.

A concept frequently present in flow cytometry, particularly when analyzing bivariate plots, is the presence of graded transitions or abrupt changes (Shapiro, 2003). These patterns in bivariate distributions are determined by the underlying biological process that is being studied. For example damage of cell membrane allows staining by PI probe so that cells may be classified as dead with a permeable membrane or live having preserved selective permeability, depending on whether they are red fluorescent or not. Cells are observed to be bright stained or having no stain at all, but very rarely they are observed to have dim red fluorescence. Thus membrane damage and PI staining is an example of an abrupt transition or discrete process represented by membrane damage that produces a sudden change in the frequency distribution. This frequency distribution is symmetric, bell-shaped, and has low variability around the peak (Fig. 1C,E.).

By contrast when analyzing drug-induced effects on esterase activity through green fluorescence we will observe a graded transition from bright fluorescence to dim fluorescence (Fig. 1C). Thus a graded biological process represented by progressively decreased esterase activity determines a skewed frequency distribution with higher variability around the peak (Fig. 1F). In this case there will be a higher probability of observing cells within any level of metabolic activity represented by the amount of green fluorescence: bright, intermediate and dim. Note also that cells with damaged membrane no longer retain fluorescein (very few events are seen in upper right quadrant, Fig. 1C).

When analysis is restricted to live cells without damaged membrane (PI negative) it is more evident that the probability of finding live cells with low metabolic activity in the drug-treated population decreases gradually (Fig. 1H). By contrast, when the analysis is restricted to cells without metabolic activity a narrow bell-shape distribution is observed meaning that the probability of finding cells with damaged membrane in cells without metabolic activity increases abruptly (Fig. 1G). When combined in a bivariate plot the gradual decrease in metabolic activity in live cells is observed as a continuous distribution or pathway, while the abrupt transition from membrane-impermeable to membrane-permeable is observed as a discrete transition to a main single cluster of PI-positive cells with very low or no metabolic activity (Fig. 1C). The probability of finding cells with low or no metabolic activity is very low as shown by the few cells in an intermediate position along this "death-pathway". Changes in FSC and SSC are also graded transitions and define a "death-pathway" in bivariate plots (Fig. 1D). Most cells having membrane damage have low FSC and high SSC, those cells without membrane damage and with metabolic activity have high FSC and low SSC, while intermediate positions may be occupied by either of these populations (Fig. 1D). Thus the death pathway defines a whole range of changes occurring in all four parameter FSC, SSC, FDA, and PI. However the main result is characterizing cells as either dead or alive and this difference is brought by PI staining and membrane damage. Thus applying quadrant analysis we would add the fraction of cells in both upper quadrants and the fraction of cells in the lower quadrants as live cells (Fig 1C). The remaining parameters will work as internal quality controls.

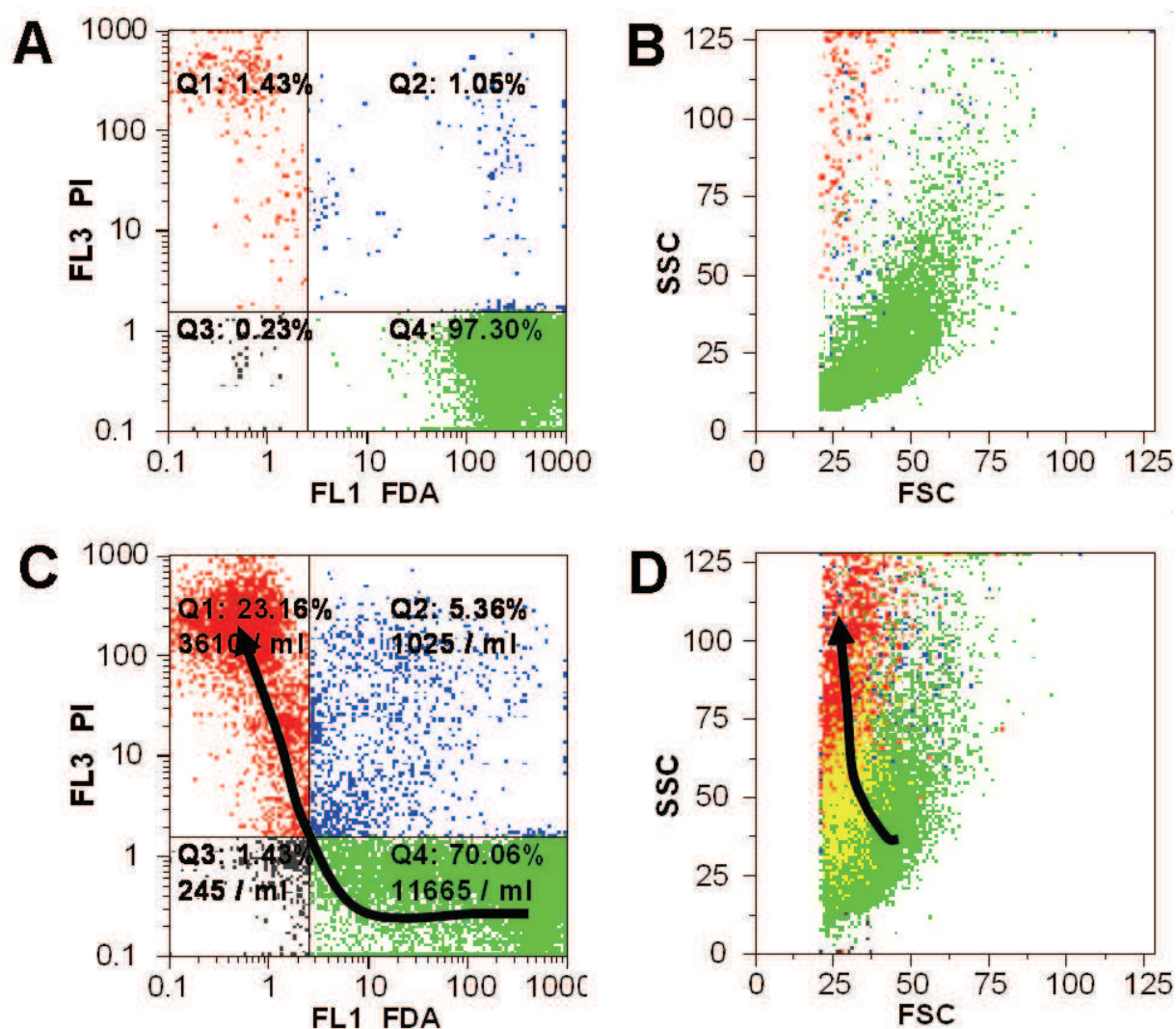


Fig. 1. (continues on next page) The FDA vs. PI bivariate plot and the cell death pathway. A. Sample of human U937 leukemic cells labelled with FDA and PI. Lower right quadrant shows that most cells (97.30%) have esterase enzymatic activity and preserved membrane permeability because they exclude PI staining. Only 1.43% of cells have PI staining without FDA fluorescence, while 1.05% are double positive indicating both enzymatic activity and damaged membrane. B. FSC-SSC profile of live cells is shown in green and corresponds to the 97.30% of cells shown in the lower right quadrant of panel A. The small amount of single PI positive (red) and double positive cells (blue) are also observed. C. Sample of human U937 cells exposed to 5 μ M sodium arsenite (AsNaO₂) for 72h stained with FDA and PI showing a "slow" transition from high FDA fluorescence to low FDA fluorescence (green) and a further "abrupt" transition to a PI positive FDA negative cluster of dead cells (red). A minority of cells are double positive (blue). The whole transition is indicated with the black arrow. D. FSC vs. SSC plot of the sample shown in C. Green color represents FSC-SSC paired values only occupied by live cells (lower right quadrant shown in C), red color represents FSC-SSC paired values only occupied by dead cells (upper left quadrant in C), while yellow color represents FSC-SSC paired values occupied by both live and dead cells. The black arrow shows the graphical death pathway transition in the FSC SSC plot. The FSC-SSC values of the minority of double positive cells are shown in blue

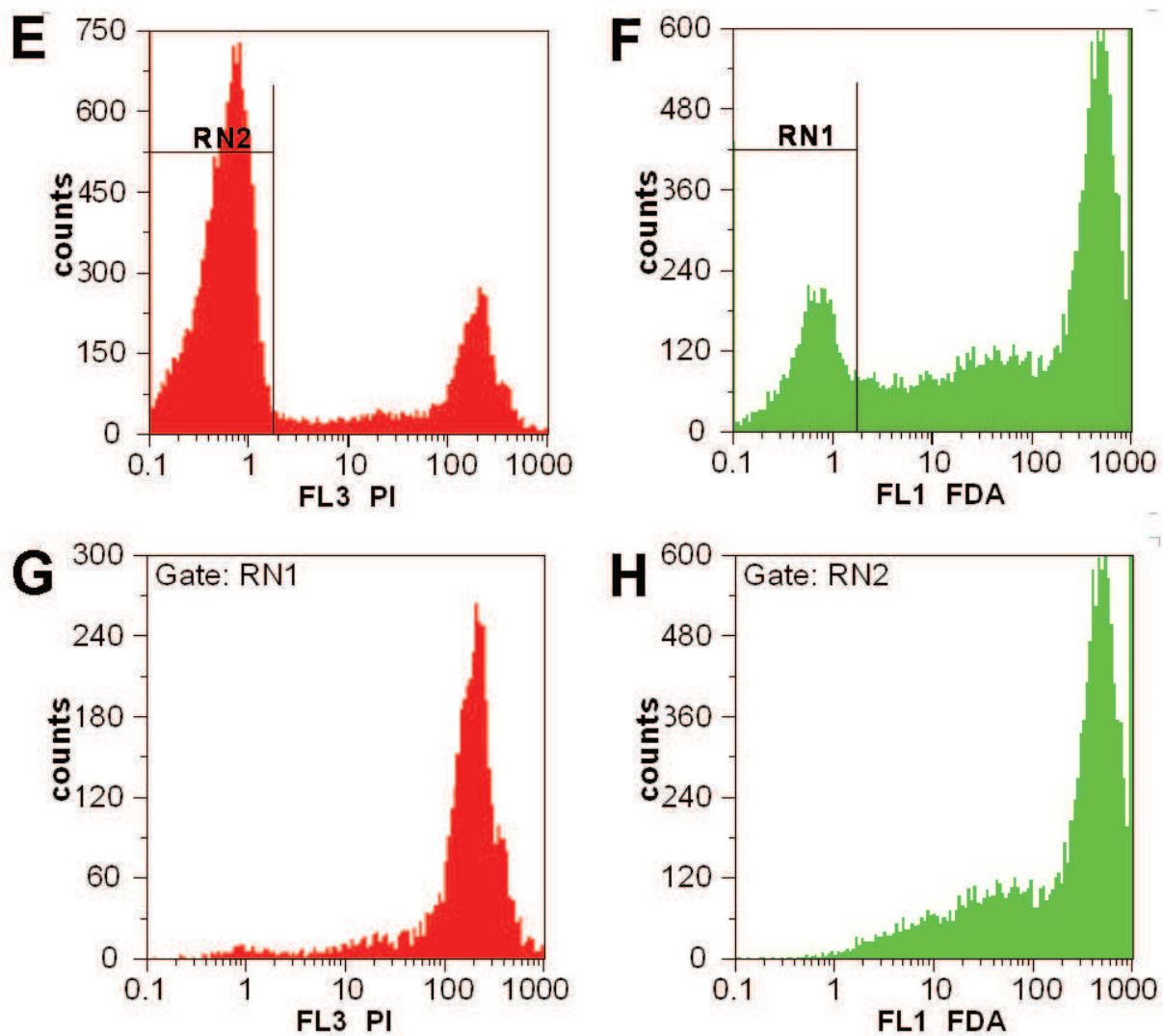


Fig. 1. (continued) E. Frequency distribution of PI fluorescence corresponding to the sample shown in C and D. Note that positive and negative cell populations are bell-shaped, symmetrical, with low variability around the peaks, and well separated from each other F. Frequency distribution of FDA fluorescence of the same sample shown in C and D. The population of positive cells shows asymmetrical left-skewed distribution with great variability to the left of the peak. G. The sample shown in E with live cells excluded. The probability of finding positive cells with intermediate and dim PI fluorescence decreases abruptly to the left. H. The sample shown in F with dead cells excluded. The probability of finding positive cells with intermediate and dim FDA fluorescence decreases slowly to the left

3. Building a cytotoxic dose response curve

Theoretically, if a population of cells were homogeneously sensitive to cell death induced by a certain drug there would be a single dose D at which 100% cell death would be observed (Casarett et al., 2008; Goodman et al., 2010). However in any given sample of drug-treated cells a random proportion of cells will die at doses lower or higher than D due to experimental and biological variability. This random divergence from D follows a Gaussian distribution (Fig. 2A,C).

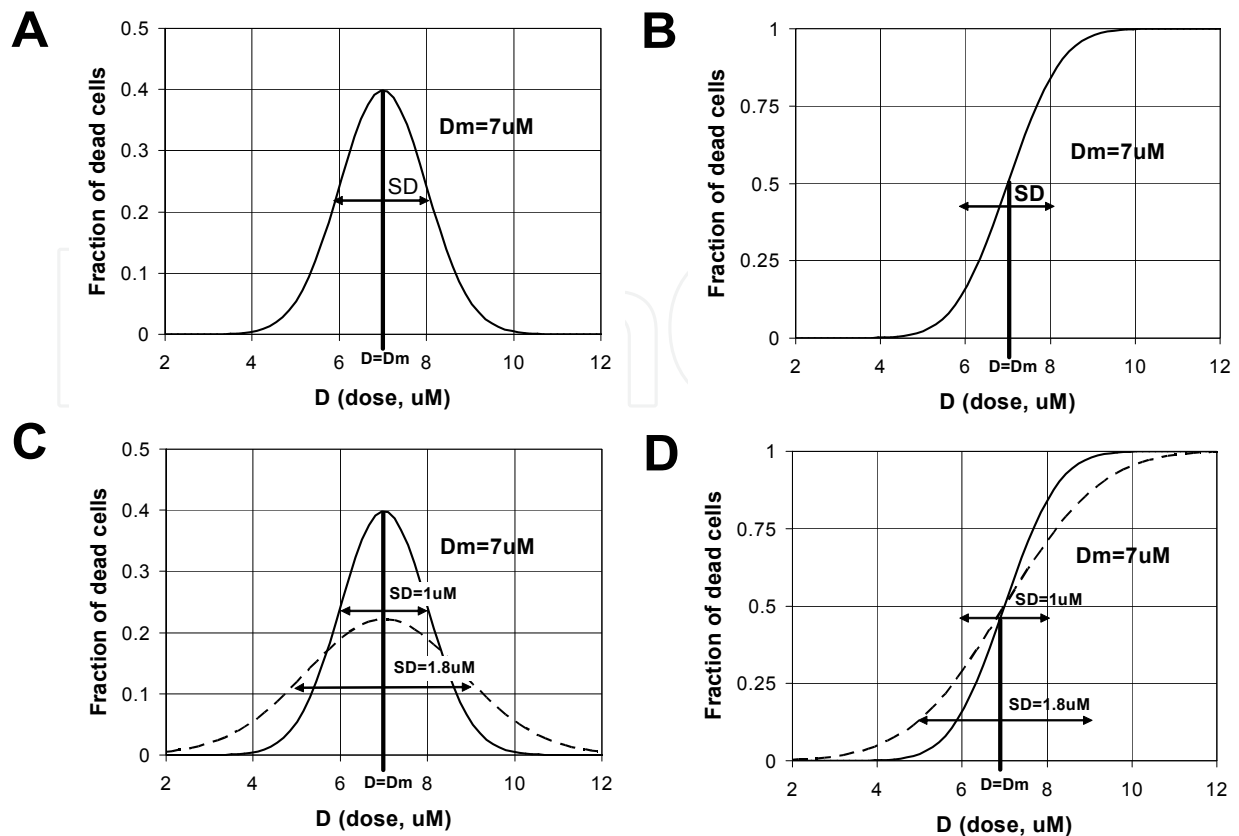


Fig. 2. Quantal dose response model. A. Single cells will show differences on the minimal drug dose required to induce cell death. D_m is the most frequent minimal dose required to elicit cell death. Variations around this value have a normal distribution. In this particular example D_m is $7\mu\text{M}$ and the standard deviation (SD) is $1\mu\text{M}$. B. D_m is the drug dose that is estimated to kill half of the cells in a sample. When running experiments exposing cells to incremental doses of a cytotoxic drug the fraction of dead cells observed will follow a normal cumulative function. C. Differences between two cytotoxic drugs in the variability observed around D_m . The drug represented by the dotted line has larger variability ($\text{SD}=1.8\mu\text{M}$) than the drug represented in full line ($\text{SD}=1\mu\text{M}$). D. Increased variability around D_m is observed as a dose response curve with a smaller slope as shown by the dotted line of the cumulative normal distribution

The median dose D_m represents a dose D where half of the cells are killed and half of the cells remain live (Fig. 2 B). However, as indicated by the bell shape of the Gaussian distribution many of the 50% of cells killed at a dose D_m may have required less than D_m to be killed. In fact as shown in figure 2A only a fraction of cells will require strictly a dose D_m (those in the bell peak), while a minority of cells will require a dose much lower than D_m to be killed (those in the left tail of the bell-shaped curve). If we conduct experiments evaluating the cytotoxic effect of increasing doses we will observe a sigmoid curve that follows a cumulative Gaussian frequency distribution (Fig. 2B). Doses lower than D_m will show decreased probability of cell death approaching 0% while doses higher than D_m will show increased probability of cell death approaching 100% (Fig. 2B). This model is known as quantal dose-response because it is based on the scoring of all members of a sample population for having or not having a certain condition at a given applied dose (Casarett et al., 2008). This is precisely what is done through flow cytometry assessing a sample on a cell

by cell basis for being dead or alive. Using flow cytometry we can measure the fraction of cells killed (f_a) at a dose D with high accuracy and precision due to the large number of cells analyzed which ensures an extremely low standard error (SE). However, high accuracy and precision apply to a single sample and not to replicates. The source of variability between replicates will be both biological and experimental. For example cells overgrown in culture may respond with higher variability than cells in exponential growth when estimated from replicates. Similarly any problems around drug exposure or the staining procedure will add to the variability of replicates although the precision and accuracy of each sample determination will be very high due to the large amount of cells scored in each sample tube. Regarding calculation of the median cytotoxic dose D_m this replicates will have a critical impact on the statistical precision of the D_m estimate.

3.1 Calculating the median dose: The median effect equation

Cells cultured in vitro can be exposed to increasing doses of a cytotoxic drug during a certain time interval (e.g., 48h or 72h) to determine a median cytotoxic dose D_m . Several doses should be tested to extend over a dose range. The lower doses should induce a fraction of dead cells close to that of unexposed cells, while the higher doses should induce death values approaching 100% or achieve a plateau of maximal effect. In between these boundary doses the more intervals assessed the more precision we will get in the estimates. For example seven doses assessed in triplicate that yield cell death fractions between 5% and 95% would be enough to obtain regression estimates with an adequate precision. The dose response sigmoidal curve can be fit to a two parameter logistic function of the type:

$$f_a = 1 / [1 + 1 / (D / D_m)^m] \quad (1)$$

where D is the dose, D_m is the dose required to achieve the median cytotoxic effect, f_a is the fraction of dead cells, and m is a measurement of the sigmoidicity of the curve. When $m=1$ the dose-effect curve is hyperbolic, when $m>1$ the curve is sigmoidal, while $m<1$ indicates a negative sigmoidal shape (Fig. 3A).

To estimate D_m and m the median effect equation is written as:

$$f_a / (1 - f_a) = (D / D_m)^m \quad (2)$$

The factor $(1 - f_a)$ is the fraction of live cells. Applying a log transformation the following linear function is obtained:

$$\log (f_a / (1 - f_a)) = m \cdot \log (D) - m \cdot \log (D_m) \quad (3)$$

Thus plotting log values of experimental doses against log values of the ratio of dead/live cells will show a linear trend that is often referred to as median effect plot (Fig. 3B).

This is a linear function of the type $y = m \cdot x + b$, where $y = f_a / (1 - f_a)$, $x = \log(D)$, and $b = -m \cdot \log(D_m)$. A linear regression can be applied to these data to obtain estimates for m and D_m . The m coefficient can be readily determined by the slope of the regression, and D_m is derived from the estimate of the intercept $-m \cdot \log(D_m)$.

The squared correlation coefficient or R^2 value is an estimate of the precision of the overall regression (Fig. 3B). In this particular application to data representing cell death vs. dose of cytotoxic drug, R^2 is affected mainly by the scattering of replicate values, which in turn

depend on the experimental and biological variability, and also on the number of sample doses in between the lowest and highest effect values. The standard error (SE) of m and the intercept can also be obtained from regression analysis to get a 95% confidence interval around $\log(D_m)$. The formula for manual calculation is rather complicated and involves computing $SE(\log(D))$ when $D=D_m$ (shown in eq. 14, Table 5) but may be obtained using any software that implements this calculation such as Calcsyn or Compusyn (Bijnsdorp et al., 2011; Ikeda et al., 2011; Ramachandran et al., 2010).

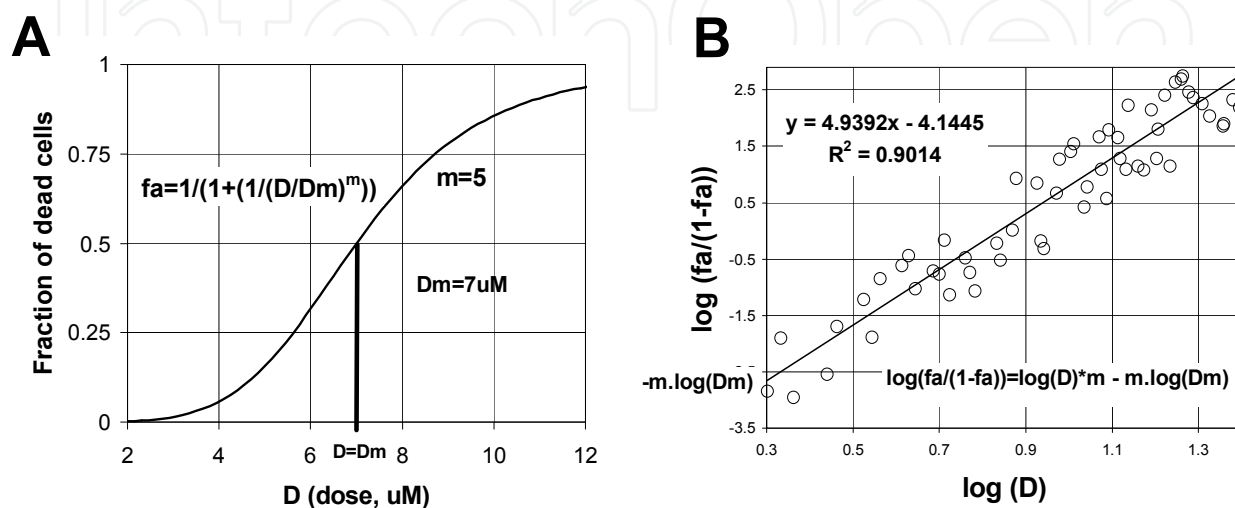


Fig. 3. Median effect plot. A. The two parameter dose-response sigmoidal curve for a particular example with $D_m=7\mu\text{M}$ and $m=5$. B. Algebraic and log transformation to obtain a linear function. A linear regression can be applied to experimental data in order to obtain estimates of the two parameters D_m and m . The squared correlation coefficient R^2 is a measure of the overall precision of the linear regression and thus the D_m and m estimates

3.2 Threshold, median dose and maximal efficacy

Analysis of the dose-effect plot can be informative about threshold values and maximal efficacy values.

In practice the threshold value will be the minimal dose where the fraction of dead cells is higher than that of untreated cells. The maximal efficacy would be the fraction of dead cells where the sigmoidal curve approaches a plateau. Quite often the maximal efficacy approaches 100%. However a cell population may exhibit a differential response and a fraction of cells may require quite larger doses. In these cases the maximal efficacy will be much less than 100%.

3.3 Comparing two drugs

To compare two drugs and evaluate whether combination results in synergy or not a first step is to calculate D_m for the two drugs. Thus, the same approach described above should be applied to the second drug. The procedure will include evaluating several doses in replicates with the same exposure time interval as the first drug, obtaining data to create a median effect plot and estimating m and D_m by linear regression (Chang et al., 1987; Chou & Talalay, 1984; Sugiyama et al., 1998).

Results from assessment of the two drugs can be analyzed together in a combined median effect plot where log doses (in molar units) are depicted against $\log(fa/1-fa)$. In this plot the relative potency of the two drugs can be easily appreciated (Fig. 4A). A drug a is said to be more potent than a second drug b regarding the cytotoxic effect when less dose of drug a is needed to achieve the same cytotoxic effect with drug b on a molar basis. In addition when the slopes of the two drugs are different it suggests that the drugs have different mechanisms to induce cytotoxicity.

The dose effect equation can be re-written to calculate the dose required to induce a given cytotoxic effect:

$$D = D_m (fa / (1-fa))^{1/m} \quad (4)$$

For example the effective cytotoxic dose 50% (EC50) is the dose D that is estimated to kill 50% of the cells. In this case $fa=0.5$ and EC50 is coincident with the median dose D_m . Similarly EC25 is the dose D that is estimated to kill 25% of the cells.

3.3.1 Assessing the combined effect of two drugs under fixed molar ratio

Once obtained the dose-response curve for two drugs a and b, a third experiment with combination of a + b will be needed to determine if the interaction of these drugs is additive, synergic or antagonistic.

Assuming that the drug b is less potent than the drug a, fixed molar ratio could be used in the combination based on the relative potency $EC50(a)/EC50(b)$. For example if $EC50(a)$ is $10\mu\text{M}$ and $EC50(b)$ is $30\mu\text{M}$, the molar ratio of the combination would be $1/3$. An empirical approach is to start the combination experiment with a combination of a+b calculated as

$$EC50(a+b) = 10^{([\log(EC50(a)) + \log(EC50(b))]/2)} \quad (5)$$

In this example this estimated value would be $17.3\mu\text{M}$. Assuming the fixed molar ratio $1/3$ this combination would have $4.3\mu\text{M}$ of drug a and $13.0\mu\text{M}$ of drug b.

Next we should treat this combination as a new drug a+b and evaluate several doses above and below $17.3\mu\text{M}$ in replicates to span a dose range of the combination. Thus, we will experimentally obtain a new data set of doses and cytotoxic effects that we should evaluate by the same procedure with the median effect plot, and conduct a linear regression to obtain estimates for m and D_m with the combination of a+b.

In particular we will obtain an effect-dose equation as shown above (eq. 4) to determine the dose of the combination a+b to achieve a desired cytotoxic effect level (EC)

$$D = D_{m_{a+b}} (fa / (1-fa))^{1/m_{a+b}} \quad (6)$$

For example applying (eq.5) $EC50(a+b)$ will be equal to the median dose estimated from the regression in the combined experiment ($D_{m_{a+b}}$)

3.4 Graphical analysis

A first approach is to plot this result together with results of single drug effects to depict some relevant information (Pegram et al., 1999). When the combined-drug curve lies in a

midpoint between the two single drug curves it suggests an additive effect (Fig. 4A). It indicates that the potency of the combined drugs is at an intermediate point between the potency of each drug. When the combined drug curve is shifted to the left it would be closer to the more potent single drug and thus suggests synergism (Fig. 1B). On the other side when the combined drug curve is shifted to the right and closer to the low potency drug it is suggestive of antagonism (Fig. 1C). Another hint that could aid in generating hypothesis is the curve shape and particularly the slope. The variability around D_m is represented by the standard deviation (SD) of the Gaussian distribution underlying the quantal dose-response model discussed above. A large SD is in accordance with a flat curve while a small SD is in accordance with a steep curve (Fig. 2C,D). This variability has a biological significance and two drugs having different mechanisms of inducing cell death in a certain cell line may have different slopes.

3.5 Calculating the combination index (CI)

The graphical analysis gives some clues about what kind of interaction results from the combination of drugs a and b and depicts useful information but is less conclusive in quantitative terms. A more thorough conclusion can be derived from computing the combination index for each cytotoxic effect level (Chou, 2008; 2010). Computing the combination index (CI) for each effect level provides an answer to what kind of interaction occurs between drug a and drug b throughout the whole dose range.

The combination index method takes data provided by single and combined dose-effect equations to provide an estimate at the whole range of cytotoxic effects. The combination index is defined for a given effect level i by the following equation:

$$CI(i) = D_{ac}(i) / D_{as}(i) + D_{bc}(i) / D_{bs}(i) + \alpha D_{ac}(i) \cdot D_{bc}(i) / D_{as}(i) \cdot D_{bs}(i) \quad (7)$$

Where $D_{ac}(i)$ and $D_{bc}(i)$ are the doses of drugs a and b respectively required in the combination a+b to produce an effect level i .

$D_{as}(i)$ and $D_{bs}(i)$ are the doses of drug a and b respectively, required to produce an effect level i when used as single drugs. For any level i , these values are obtained from the three dose response curves defined by (eq. 4) (two single and one combined) obtained with parameters D_m and m that in turn were obtained from regression analysis with (eq.3) applied to experimental data. It is often assumed the conservative criteria that cytotoxic drugs are mutually non exclusive and $\alpha=1$. If the three lines are strictly parallel and both drugs have a similar molecular target it could be assumed that they are mutually exclusive and in that case $\alpha=0$. If the fixed molar ratio of drug a and b in the combined treatment is p/q , then for an effect level i :

$$D_{as}(i) = D_{m_a} (f_a(i) / (1 - f_a(i)))^{1/m_a} \quad (8)$$

$$D_{bs}(i) = D_{m_b} (f_b(i) / (1 - f_b(i)))^{1/m_b} \quad (9)$$

$$D_{ac}(i) = p / (p + q) D_{m_{a+b}} (f_a(i) / (1 - f_a(i)))^{1/m_{a+b}} \quad (10)$$

$$D_{bc}(i) = q / (p + q) D_{m_{a+b}} (f_b(i) / (1 - f_b(i)))^{1/m_{a+b}} \quad (11)$$

Where $fa(i)$ is the fraction of dead cells at effect level i , Dm_a and m_a are the median dose and the slope estimated for drug a , Dm_b and m_b are the median dose and the slope estimated for drug b , and Dm_{a+b} and m_{a+b} are the median dose and the slope estimated for the combined treatment with drugs a and b . Thus the combination index is calculated for any effect level above 0 and below 1.

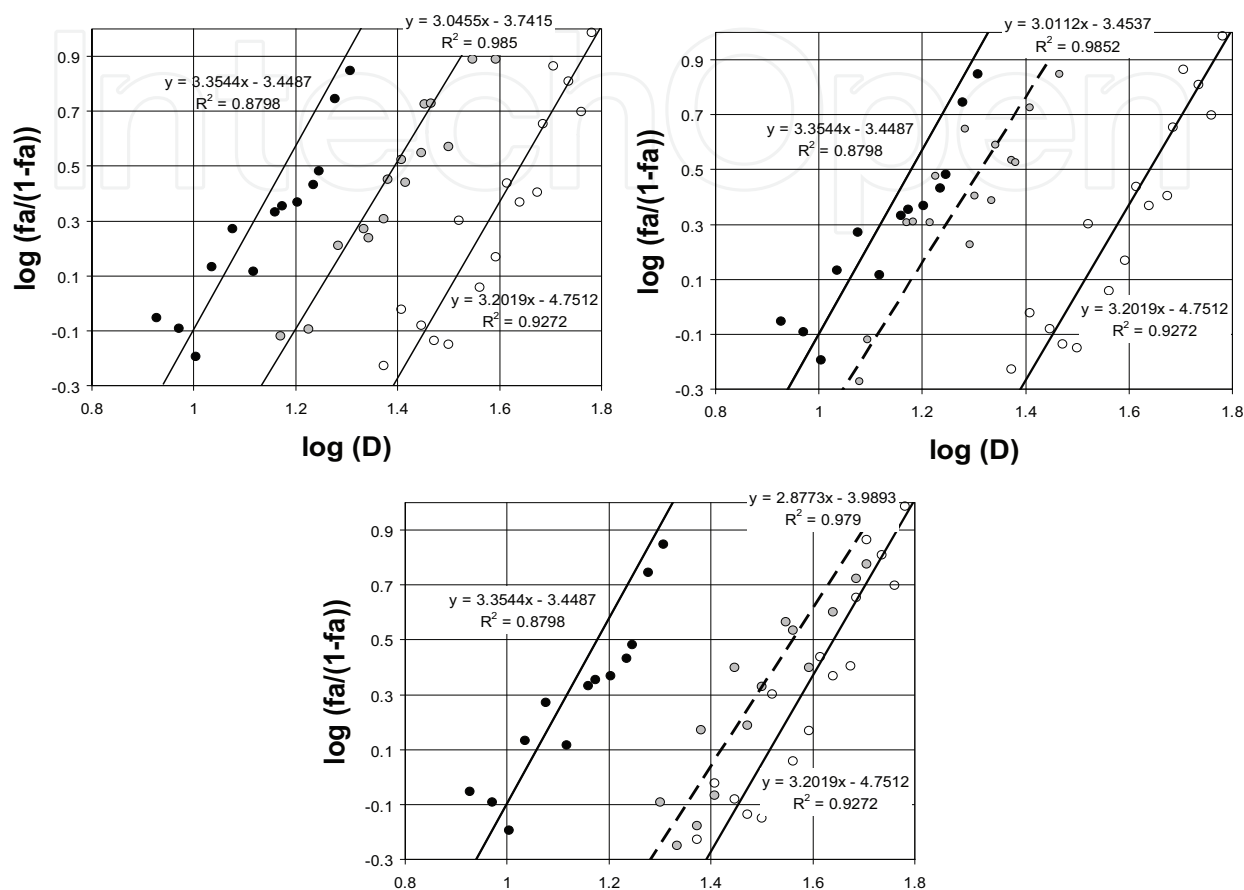


Fig. 4. Drug interaction and median effect plot. A. In this example experimental values are represented by circles and linear regression is applied to obtain estimates for Dm and m . Experimental values obtained for a drug a are shown in black circles. The values of Dm and m for drug a were $10 \mu\text{M}$ and 3.0 respectively. Experimental values for a less potent drug b are shown in open circles. The values of Dm and m for drug b were $30 \mu\text{M}$ and 3.0 respectively. A combined experiment was run with $a+b$ with a constant mass ratio of $1/3$ based on $EC50(a)/EC50(b)$ and assuming that under additive effect $EC50(a+b) = 10\{[\log(EC50(a)) + \log(EC50(b))]/2\}$. Experimental values for the combination are shown in grey circles. The values of Dm and m for the combination $a+b$ were $17.0 \mu\text{M}$ and 3.0 respectively. In this example drugs a and b have an additive interaction and the median effect plot of the combination lies in a mid position between the lines corresponding to the single drugs. B. The same experiment shown in A, but in this case the drugs a and b have synergistic effect. The values of Dm and m for the combination $a+b$ were $14.0 \mu\text{M}$ and 3.0 respectively. The median effect plot of the combination is shifted towards the drug a , which has the highest potency. C. The same experiment shown in A, but in this example the drugs a and b have antagonistic effect. The values of Dm and m for the combination $a+b$ were $24.4 \mu\text{M}$ and 2.9 respectively. The median effect plot of the combination in this case is shifted towards the drug b which has the lowest potency

			Three alternative results of the experimental assay with combination a + b (considering $\alpha=1$, mutually non-exclusive condition)		
			Additive	Synergic	Antagonistic
	Single drug a	Single drug b	Combined drugs a+b	Combined drugs a+b	Combined drugs a+b
Dm (uM) ^{#(1)}	10	30	17	14	24.4
m ^{#(1)}	3	3	3	3	3
fa(i)	0.5				
Das(i) ^{#(2)}	10				
Dbs(i) ^{#(3)}		30			
Dac(i) ^{#(4)}			4.25	3.5	6.1
Dbc(i) ^{#(5)}			12.75	10.5	18.3
p/(p+q) ^{#(6)}			0.25	0.25	0.25
q/(p+q) ^{#(6)}			0.75	0.75	0.75
CI (i) ^{#(7)}			1.03	0.82	1.59
$SE(CI(i)) = \left\{ \left[\frac{Dac(i)}{Das(i)} \cdot \left[SE(Dac(i)/Dac(i) + SE(Das(i)/Das(i)) \right]^2 + \left[\frac{Dbc(i)}{Dbs(i)} \cdot \left[SE(Dbc(i)/Dbc(i) + SE(Dbs(i)/Dbs(i)) \right]^2 \right] \right\}^{1/2}$ <p style="text-align: right;">(eq. 12)</p>					
$SE(D) = 1/2 \cdot \left\{ 10^{\left[\log(D) + SE(\log(D)) \right]} - 10^{\left[\log(D) - SE(\log(D)) \right]} \right\}$ <p style="text-align: right;">(eq. 13)</p>					
$SE(\log(D)) = \left\{ \log(D) \cdot \left[SE(b)/\log(fa/(1-fa)-b) \right]^2 + \left[SE(m)/m \right]^2 + 2 \left[-(\log D)^{1/2} \cdot SE(m)/SE(b) \right] \cdot SE(b)/b \cdot SE(m)/m \right\}^{1/2}$ <p style="text-align: right;">(eq. 14)</p>					
where $b = -m \cdot \log(Dm)$					
A 95% confidence interval around D in general and around Dm in particular, can be computed using the formulas for standard error (SE, eq. 13 and eq. 14).					
A 95% confidence interval around CI at any effect level i can be computed from the standard error formulas presented in eq. 12, 13, and 14.					

(1) Obtained from linear regression of experimental data

(2) $Das(i) = Dm_a \cdot (fa(i)/(1-fa(i)))^{1/m_a}$

(3) $Dbs(i) = Dm_b \cdot (fa(i)/(1-fa(i)))^{1/m_b}$

(4) $Dac(i) = p/(p+q) \cdot Dm_{a+b} \cdot (fa(i)/(1-fa(i)))^{1/m_{a+b}}$

(5) $Dbc(i) = q/(p+q) \cdot Dm_{a+b} \cdot (fa(i)/(1-fa(i)))^{1/m_{a+b}}$

(6) Molar ratio $p/q = Dm(a) / Dm(b) = 10/30 = 1/3$

(7) $CI(i) = Dac(i) / Das(i) + Dbc(i) / Dbs(i) + \alpha \cdot Dac(i) \cdot Dbc(i) / Das(i) \cdot Dbs(i)$

Table 5. CI calculation between two drugs a and b at the 50% effect level under three alternative conditions: additive, synergic, antagonistic. To obtain CI as a function of the effect level i, the calculation has to be repeated for each arbitrary level i between 0 and 1. A 95% confidence interval around D in general and around Dm in particular, can be computed using the formulas for standard error (SE, eq. 13 and eq. 14). A 95% confidence interval around CI at any effect level i can be computed from the standard error formulas presented in eq. 12, 13 and 14

Table 5 summarizes a manual calculation of CI of two drugs a and b using these formulas for the 50% effect level under three hypothetical results: additive, synergic or antagonistic effect.

The same calculation can be applied to any effect level to plot CI as a function of effect level. When the interaction is additive CI =1. In this case it can be interpreted that one of the drugs (the less potent one, i.e. drug b in the example) is acting as though it is merely a diluted form of the other (drug a in the example). When CI<1 the combination of a+b is synergic while CI>1 indicates antagonism. Synergy, implies that the combination of the two drugs achieves a cytotoxic effect greater than that expected by the simple addition of the effects of the drugs a and b, while antagonism achieves a cytotoxic effect lower than that expected by additive effects of drugs a and b.

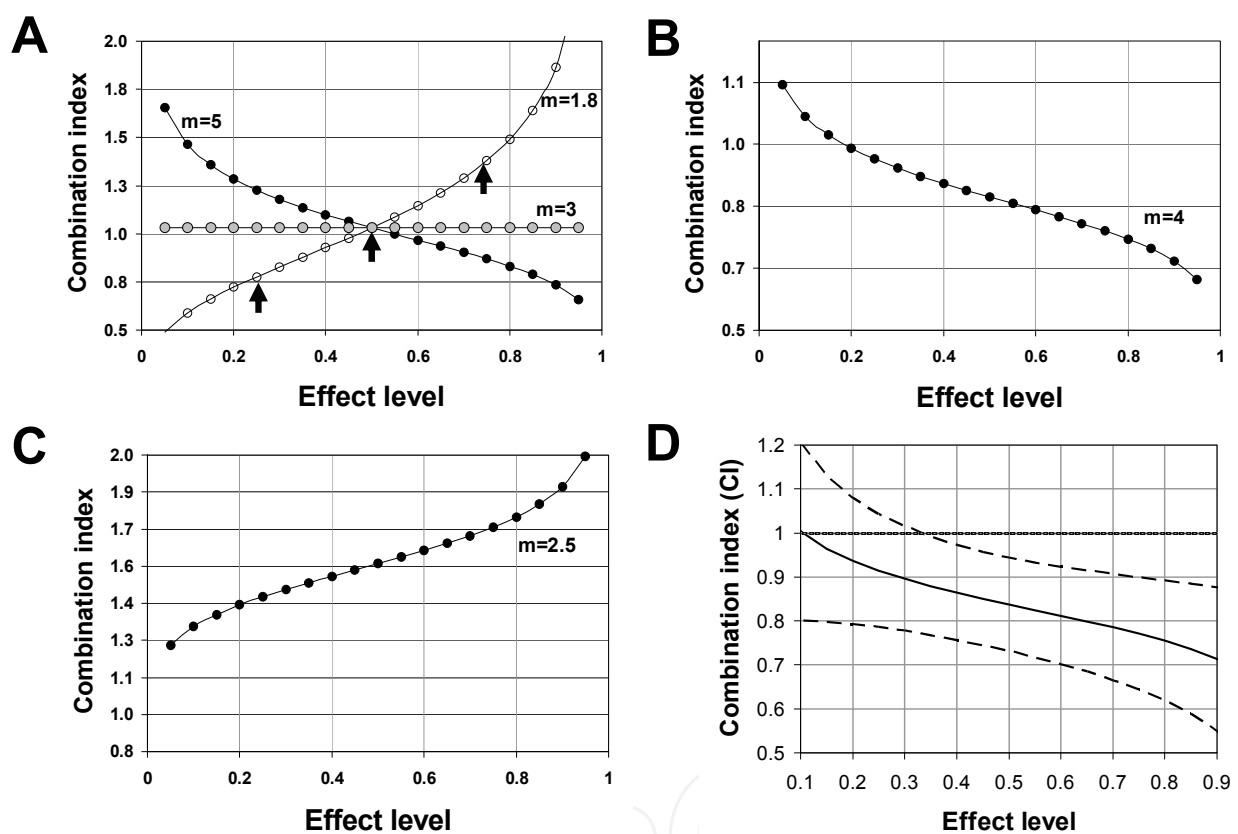


Fig. 5. Drug interaction and CI calculation. A. Only rarely the combination index obtained is constant for all effect levels. Here it is shown how different values of the slope m obtained through linear regression in the combination experiment (a+b) would affect the shape of the curve representing the CI as a function of the effect level. Similarly, differences between the slopes obtained for drugs a and b through the single drug experiments will contribute to the uneven shape of the CI function. Note that depending on the effect level the interaction a+b with $m=1.8$ would be synergism, additive or antagonism at EC25, EC50, and EC75 respectively (arrows). B. Results of CI calculation for the example where a+b results in synergism considering $m=4$ in the regression of the combined-drug experiment. C. Results of CI calculation for the example where a+b results in antagonism considering $m=2.5$ in the regression of the combined-drug experiment. D. 95% confidence level intervals around CI, using an algebraic approximation (eq. 12, Table 5) in an example where combination of a+b is synergic

The horizontal line corresponding to $CI(i)=1$, where i is any effect level in the interval $(0,1)$, is often called the additive effect line. A combination of drugs a and b may result in CI values above or below the additive line at different effect levels. Thus, the CI as a function of effect level is not constant or linear and it may be decreasing or increasing (Fig 5A). If data from the combination experiment in the example of figure 4A resulted in $m_{a+b}=5$ or $m_{a+b}=1.8$, even still with $Dm_{a+b}=17$ the CI line would be inclined downwards or upwards respectively (Fig. 5A). Only at effect levels close to EC_{50} the result would be strictly additive. An important conclusion is that for some drug combinations, experiments conducted at different single dose-effect levels may yield opposing results. For example if the combination $a+b$ with $m=1.8$ shown in figure 5A were experimentally evaluated only at effect level 0.25 the single dose analysis would conclude on synergism. However if it were evaluated at effect level 0.75 it would conclude on antagonism (Fig. 5A). This exemplifies why the assessment of combination index over the whole dose range will show all kinds of interactions that may result from combination at different effect levels.

Computing a standard error of CI allows plotting confidence intervals at all effect levels providing a further assurance over the computation. A 95% confidence interval will indicate that if we repeat the experiment 100 times, 95 out of 100 times the CI would be within this interval. For example, observing whether or not confidence limits are above or below the additive line will allow concluding with further statistical support on antagonism or synergism respectively. Computation of the standard error of CI and confidence intervals at all levels should be better obtained through specialized software such as Calcsyn or Compusyn (Bijnsdorp et al., 2011; Chou, 2010). It may also require approaches such as Monte Carlo simulation based on the estimated parameter for m and Dm in single and combined equations.

4. Concluding remarks

A thorough assessment of drug interaction is an essential step in targeted combined therapy. The new targeted agents are seldom useful as single agents but may be effective when used in specific combinations. The median effect and combination index calculation are well founded methods traditionally used in pharmacological and toxicological studies. Since new cytotoxic drugs target mechanisms eliciting cell death, biomarkers related to viability assessment are preferred to biomarkers of cell proliferation. Flow cytometry is an ideal technology to provide massive data from cell death biomarkers to build dose response curves of cytotoxic effect. When these data is further used to determine the combination index a full characterization of drug interaction over the cytotoxic effect is obtained at all effect levels. This approach can be applied to tumor cell lines in preclinical studies and also in patient-derived tumor cells, thus providing useful information as prospective indicators of the potential therapeutic response to combined-drug antitumor treatment.

5. References

- Armand, J. P., Burnett, A. K., Drach, J., Harousseau, J. L., Lowenberg, B. & San Miguel, J. (2007). The emerging role of targeted therapy for hematologic malignancies: update on bortezomib and tipifarnib. *Oncologist* Vol. 12, No. 3, (Mar, 2007), pp. 281-290

- Barnett, M. J., McGhee-Wilson, D., Shapiro, A. M. & Lakey, J. R. (2004). Variation in human islet viability based on different membrane integrity stains. *Cell Transplant* Vol. 13, No. 5, (2004), pp. 481-488
- Belinsky, S. A., Grimes, M. J., Picchi, M. A., Mitchell, H. D., Stidley, C. A., Tesfaigzi, Y., Channell, M. M., Liu, Y., Casero, R. A., Jr., Baylin, S. B. et al. (2011). Combination therapy with vidaza and entinostat suppresses tumor growth and reprograms the epigenome in an orthotopic lung cancer model. *Cancer Res* Vol. 71, No. 2, (Jan 15, 2011), pp. 454-462
- Berghe, T. V., Vanlangenakker, N., Parthoens, E., Deckers, W., Devos, M., Festjens, N., Guerin, C. J., Brunk, U. T., Declercq, W. & Vandenamele, P. (2010). Necroptosis, necrosis and secondary necrosis converge on similar cellular disintegration features. *Cell Death Differ* Vol. 17, No. 6, (Jun, 2010), pp. 922-930
- Bijnsdorp, I. V., Giovannetti, E. & Peters, G. J. (2011). Analysis of drug interactions. *Methods Mol Biol* Vol. 731, No., (2011), pp. 421-434
- Boccardo, M., Morgan, G. & Cavenagh, J. (2005). Preclinical evaluation of the proteasome inhibitor bortezomib in cancer therapy. *Cancer Cell Int* Vol. 5, No. 1, (Jun 1, 2005), pp. 18
- Bross, P. F., Kane, R., Farrell, A. T., Abraham, S., Benson, K., Brower, M. E., Bradley, S., Gobburu, J. V., Goheer, A., Lee, S. L. et al. (2004). Approval summary for bortezomib for injection in the treatment of multiple myeloma. *Clin Cancer Res* Vol. 10, No. 12 Pt 1, (Jun 15, 2004), pp. 3954-3964
- Burmeister, Y., Lischke, T., Dahler, A. C., Mages, H. W., Lam, K. P., Coyle, A. J., Kroczek, R. A. & Hutloff, A. (2008). ICOS controls the pool size of effector-memory and regulatory T cells. *J Immunol* Vol. 180, No. 2, (Jan 15, 2008), pp. 774-782
- Busch, C., Geisler, J., Knappskog, S., Lillehaug, J. R. & Lonning, P. E. Alterations in the p53 pathway and p16INK4a expression predict overall survival in metastatic melanoma patients treated with dacarbazine. *J Invest Dermatol* Vol. 130, No. 10, (Oct, pp. 2514-2516
- Callewaert, D. M., Radcliff, G., Waite, R., LeFevre, J. & Poulik, M. D. (1991). Characterization of effector-target conjugates for cloned human natural killer and human lymphokine activated killer cells by flow cytometry. *Cytometry* Vol. 12, No. 7, (1991), pp. 666-676
- Cameron, D. A., Ritchie, A. A. & Miller, W. R. (2001). The relative importance of proliferation and cell death in breast cancer growth and response to tamoxifen. *Eur J Cancer* Vol. 37, No. 12, (Aug, 2001), pp. 1545-1553
- Carew, J. S., Giles, F. J. & Nawrocki, S. T. (2008). Histone deacetylase inhibitors: mechanisms of cell death and promise in combination cancer therapy. *Cancer Lett* Vol. 269, No. 1, (Sep 28, 2008), pp. 7-17
- Casarett, L. J., Doull, J. & Klaassen, C. D. (2008). *Casarett and Doull's toxicology: the basic science of poisons*. 7th Edition. McGraw-Hill. ISBN (9780071470513-0071470514) New York
- Castaneda, C. A. & Gomez, H. L. (2009). Targeted therapies: Combined lapatinib and paclitaxel in HER2-positive breast cancer. *Nat Rev Clin Oncol* Vol. 6, No. 6, (Jun, 2009), pp. 308-309

- Citri, A., Kochupurakkal, B. S. & Yarden, Y. (2004). The achilles heel of ErbB-2/HER2: regulation by the Hsp90 chaperone machine and potential for pharmacological intervention. *Cell Cycle* Vol. 3, No. 1, (Jan, 2004), pp. 51-60
- Czekanska, E. M. (2011). Assessment of cell proliferation with resazurin-based fluorescent dye. *Methods Mol Biol* Vol. 740, No., 2011), pp. 27-32
- Chang, T. T., Gulati, S., Chou, T. C., Colvin, M. & Clarkson, B. (1987). Comparative cytotoxicity of various drug combinations for human leukemic cells and normal hematopoietic precursors. *Cancer Res* Vol. 47, No. 1, (Jan 1, 1987), pp. 119-122
- Chou, T. C. (2008). Preclinical versus clinical drug combination studies. *Leuk Lymphoma* Vol. 49, No. 11, (Nov, 2008), pp. 2059-2080
- Chou, T. C. (2010). Drug combination studies and their synergy quantification using the Chou-Talalay method. *Cancer Res* Vol. 70, No. 2, (Jan 15, 2010), pp. 440-446
- Chou, T. C. & Talalay, P. (1984). Quantitative analysis of dose-effect relationships: the combined effects of multiple drugs or enzyme inhibitors. *Adv Enzyme Regul* Vol. 22, No., 1984), pp. 27-55
- Dai, Y., Rahmani, M. & Grant, S. (2003). Proteasome inhibitors potentiate leukemic cell apoptosis induced by the cyclin-dependent kinase inhibitor flavopiridol through a SAPK/JNK- and NF-kappaB-dependent process. *Oncogene* Vol. 22, No. 46, (Oct 16, 2003), pp. 7108-7122
- Dancey, J. E. & Chen, H. X. (2006). Strategies for optimizing combinations of molecularly targeted anticancer agents. *Nat Rev Drug Discov* Vol. 5, No. 8, (Aug, 2006), pp. 649-659
- Darzynkiewicz, Z., Traganos, F., Staiano-Coico, L., Kapuscinski, J. & Melamed, M. R. (1982). Interaction of rhodamine 123 with living cells studied by flow cytometry. *Cancer Res* Vol. 42, No. 3, (Mar, 1982), pp. 799-806
- De Clerck, L. S., Bridts, C. H., Mertens, A. M., Moens, M. M. & Stevens, W. J. (1994). Use of fluorescent dyes in the determination of adherence of human leucocytes to endothelial cells and the effect of fluorochromes on cellular function. *J Immunol Methods* Vol. 172, No. 1, (Jun 3, 1994), pp. 115-124
- Derenzini, M., Brighenti, E., Donati, G., Vici, M., Ceccarelli, C., Santini, D., Taffurelli, M., Montanaro, L. & Trere, D. (2009). The p53-mediated sensitivity of cancer cells to chemotherapeutic agents is conditioned by the status of the retinoblastoma protein. *J Pathol* Vol. 219, No. 3, (Nov, 2009), pp. 373-382
- Dive, C., Gregory, C. D., Phipps, D. J., Evans, D. L., Milner, A. E. & Wyllie, A. H. (1992). Analysis and discrimination of necrosis and apoptosis (programmed cell death) by multiparameter flow cytometry. *Biochim Biophys Acta* Vol. 1133, No. 3, (Feb 3, 1992), pp. 275-285
- Duan, X. F., Wu, Y. L., Xu, H. Z., Zhao, M., Zhuang, H. Y., Wang, X. D., Yan, H. & Chen, G. Q. (2010). Synergistic mitosis-arresting effects of arsenic trioxide and paclitaxel on human malignant lymphocytes. *Chem Biol Interact* Vol. 183, No. 1, (Jan 5, 2010), pp. 222-230
- Elrefaei, M., Baker, C. A., Jones, N. G., Bangsberg, D. R. & Cao, H. (2008). Presence of suppressor HIV-specific CD8+ T cells is associated with increased PD-1 expression on effector CD8+ T cells. *J Immunol* Vol. 180, No. 11, (Jun 1, 2008), pp. 7757-7763
- Eray, M., Matto, M., Kaartinen, M., Andersson, L. & Pelkonen, J. (2001). Flow cytometric analysis of apoptotic subpopulations with a combination of annexin V-FITC,

- propidium iodide, and SYTO 17. *Cytometry* Vol. 43, No. 2, (Feb 1, 2001), pp. 134-142
- Eriksen, K. W., Sondergaard, H., Woetmann, A., Krejsgaard, T., Skak, K., Geisler, C., Wasik, M. A. & Odum, N. (2009). The combination of IL-21 and IFN-alpha boosts STAT3 activation, cytotoxicity and experimental tumor therapy. *Mol Immunol* Vol. 46, No. 5, (Feb, 2009), pp. 812-820
- Eruslanov, E. & Kusmartsev, S. (2010). Identification of ROS using oxidized DCFDA and flow-cytometry. *Methods Mol Biol* Vol. 594, No., (2010), pp. 57-72
- Facoetti, A., Ranza, E. & Nano, R. (2008). Proliferation and programmed cell death: role of p53 protein in high and low grade astrocytoma. *Anticancer Res* Vol. 28, No. 1A, (Jan-Feb, 2008), pp. 15-19
- Favoni, R. E. & Florio, T. (2011). Combined chemotherapy with cytotoxic and targeted compounds for the management of human malignant pleural mesothelioma. *Trends Pharmacol Sci* Vol. 32, No. 8, (Aug, 2011), pp. 463-479
- Foye, W. O. (1995). *Cancer chemotherapeutic agents*. American Chemical Society. ISBN (9780841229204-0841229201) Washington, DC
- Fuchs, T. A., Abed, U., Goosmann, C., Hurwitz, R., Schulze, I., Wahn, V., Weinrauch, Y., Brinkmann, V. & Zychlinsky, A. (2007). Novel cell death program leads to neutrophil extracellular traps. *J Cell Biol* Vol. 176, No. 2, (Jan 15, 2007), pp. 231-241
- Fujioka, H., Hunt, P. J., Rozga, J., Wu, G. D., Cramer, D. V., Demetriou, A. A. & Moscioni, A. D. (1994). Carboxyfluorescein (CFSE) labelling of hepatocytes for short-term localization following intraportal transplantation. *Cell Transplant* Vol. 3, No. 5, (Sep-Oct, 1994), pp. 397-408
- Goodman, L. S., Brunton, L. L., Chabner, B. & Knollmann, B. C. (2010). *Goodman & Gilman's pharmacological basis of therapeutics*. 12th Edition. McGraw-Hill. ISBN (9780071624428-0071624422) New York
- Gozuacik, D. & Kimchi, A. (2007). Autophagy and cell death. *Curr Top Dev Biol* Vol. 78, No., (2007), pp. 217-245
- Gross-Goupil, M. & Escudier, B. (2010). [Targeted therapies: sequential and combined treatments]. *Bull Cancer* Vol. 97, No., (2010), pp. 65-71
- Haase, S. B. (2004). Cell cycle analysis of budding yeast using SYTOX Green. *Curr Protoc Cytom* Vol. Chapter 7, No., (Nov, 2004), pp. Unit 7 23
- Hamilton, D., Loignon, M., Alaoui-Jamali, M. A. & Batist, G. (2007). Novel use of the fluorescent dye 5-(and-6)-chloromethyl SNARF-1 acetate for the measurement of intracellular glutathione in leukemic cells and primary lymphocytes. *Cytometry A* Vol. 71, No. 9, (Sep, 2007), pp. 709-715
- Healy, E., Dempsey, M., Lally, C. & Ryan, M. P. (1998). Apoptosis and necrosis: mechanisms of cell death induced by cyclosporine A in a renal proximal tubular cell line. *Kidney Int* Vol. 54, No. 6, (Dec, 1998), pp. 1955-1966
- Ikeda, H., Taira, N., Nogami, T., Shien, K., Okada, M., Shien, T., Doihara, H. & Miyoshi, S. (2011). Combination treatment with fulvestrant and various cytotoxic agents (doxorubicin, paclitaxel, docetaxel, vinorelbine, and 5-fluorouracil) has a synergistic effect in estrogen receptor-positive breast cancer. *Cancer Sci* Vol., No., (Jul 30, 2011),

- Jones, K. H. & Senft, J. A. (1985). An improved method to determine cell viability by simultaneous staining with fluorescein diacetate-propidium iodide. *J Histochem Cytochem* Vol. 33, No. 1, (Jan, 1985), pp. 77-79
- Kane, R. C., Dagher, R., Farrell, A., Ko, C. W., Sridhara, R., Justice, R. & Pazdur, R. (2007). Bortezomib for the treatment of mantle cell lymphoma. *Clin Cancer Res* Vol. 13, No. 18 Pt 1, (Sep 15, 2007), pp. 5291-5294
- Karaca, B., Atmaca, H., Uzunoglu, S., Karabulut, B., Sanli, U. A. & Uslu, R. (2009). Enhancement of taxane-induced cytotoxicity and apoptosis by gossypol in human breast cancer cell line MCF-7. *J Buon* Vol. 14, No. 3, (Jul-Sep, 2009), pp. 479-485
- Karp, J. E. & Lancet, J. E. (2005). Development of the farnesyltransferase inhibitor tipifarnib for therapy of hematologic malignancies. *Future Oncol* Vol. 1, No. 6, (Dec, 2005), pp. 719-731
- Kim, D., Cheng, G. Z., Lindsley, C. W., Yang, H. & Cheng, J. Q. (2005). Targeting the phosphatidylinositol-3 kinase/Akt pathway for the treatment of cancer. *Curr Opin Investig Drugs* Vol. 6, No. 12, (Dec, 2005), pp. 1250-1258
- Klosowska-Wardega, A., Hasumi, Y., Ahgren, A., Heldin, C. H. & Hellberg, C. (2010). Combination therapy using imatinib and vatalanib improves the therapeutic efficiency of paclitaxel towards a mouse melanoma tumor. *Melanoma Res* Vol., No., (Oct 21, 2010),
- Lantz, R. C., Lemus, R., Lange, R. W. & Karol, M. H. (2001). Rapid reduction of intracellular glutathione in human bronchial epithelial cells exposed to occupational levels of toluene diisocyanate. *Toxicol Sci* Vol. 60, No. 2, (Apr, 2001), pp. 348-355
- Larsen, A. K., Ouaret, D., El Ouadrani, K. & Petitprez, A. (2011). Targeting EGFR and VEGF(R) pathway cross-talk in tumor survival and angiogenesis. *Pharmacol Ther* Vol. 131, No. 1, (Jul, 2011), pp. 80-90
- Lebaron, P., Catala, P. & Parthuisot, N. (1998). Effectiveness of SYTOX Green stain for bacterial viability assessment. *Appl Environ Microbiol* Vol. 64, No. 7, (Jul, 1998), pp. 2697-2700
- Li, X., Dancausse, H., Grijalva, I., Oliveira, M. & Levi, A. D. (2003). Labeling Schwann cells with CFSE-an in vitro and in vivo study. *J Neurosci Methods* Vol. 125, No. 1-2, (May 30, 2003), pp. 83-91
- Marchetti, C., Jouy, N., Leroy-Martin, B., Defosse, A., Formstecher, P. & Marchetti, P. (2004). Comparison of four fluorochromes for the detection of the inner mitochondrial membrane potential in human spermatozoa and their correlation with sperm motility. *Hum Reprod* Vol. 19, No. 10, (Oct, 2004), pp. 2267-2276
- McCall, K. (2010). Genetic control of necrosis - another type of programmed cell death. *Curr Opin Cell Biol* Vol. 22, No. 6, (Dec, 2010), pp. 882-888
- Michiels, S., Potthoff, R. F. & George, S. L. (2011). Multiple testing of treatment-effect-modifying biomarkers in a randomized clinical trial with a survival endpoint. *Stat Med* Vol. 30, No. 13, (Jun 15, 2011), pp. 1502-1518
- Mitsiades, C. S., Davies, F. E., Laubach, J. P., Joshua, D., San Miguel, J., Anderson, K. C. & Richardson, P. G. (2011). Future directions of next-generation novel therapies, combination approaches, and the development of personalized medicine in myeloma. *J Clin Oncol* Vol. 29, No. 14, (May 10, 2011), pp. 1916-1923
- Mueller, M. T., Hermann, P. C., Witthauer, J., Rubio-Viqueira, B., Leicht, S. F., Huber, S., Ellwart, J. W., Mustafa, M., Bartenstein, P., D'Haese, J. G. et al. (2009). Combined

- targeted treatment to eliminate tumorigenic cancer stem cells in human pancreatic cancer. *Gastroenterology* Vol. 137, No. 3, (Sep, 2009), pp. 1102-1113
- Notte, A., Leclere, L. & Michiels, C. (2011). Autophagy as a mediator of chemotherapy-induced cell death in cancer. *Biochem Pharmacol* Vol. 82, No. 5, (Sep 1, 2011), pp. 427-434
- Olszewska-Slonina, D., Drewa, T., Musialkiewicz, D. & Olszewski, K. (2004). Comparison of viability of B16 and CI S91 cells in three cytotoxicity tests: cells counting, MTT and flow cytometry after cytostatic drug treatment. *Acta Pol Pharm* Vol. 61, No. 1, (Jan-Feb, 2004), pp. 31-37
- Paglin, S., Lee, N. Y., Nakar, C., Fitzgerald, M., Plotkin, J., Deuel, B., Hackett, N., McMahon, M., Sphicas, E., Lampen, N. et al. (2005). Rapamycin-sensitive pathway regulates mitochondrial membrane potential, autophagy, and survival in irradiated MCF-7 cells. *Cancer Res* Vol. 65, No. 23, (Dec 1, 2005), pp. 11061-11070
- Pallis, M., Syan, J. & Russell, N. H. (1999). Flow cytometric chemosensitivity analysis of blasts from patients with acute myeloblastic leukemia and myelodysplastic syndromes: the use of 7AAD with antibodies to CD45 or CD34. *Cytometry* Vol. 37, No. 4, (Dec 1, 1999), pp. 308-313
- Papadopoulos, N. G., Dedoussis, G. V., Spanakos, G., Gritzapis, A. D., Baxevanis, C. N. & Papamichail, M. (1994). An improved fluorescence assay for the determination of lymphocyte-mediated cytotoxicity using flow cytometry. *J Immunol Methods* Vol. 177, No. 1-2, (Dec 28, 1994), pp. 101-111
- Parish, C. R. & Warren, H. S. (2002). Use of the intracellular fluorescent dye CFSE to monitor lymphocyte migration and proliferation. *Curr Protoc Immunol* Vol. Chapter 4, No., (Aug, 2002), pp. Unit 4 9
- Pegram, M., Hsu, S., Lewis, G., Pietras, R., Beryt, M., Sliwkowski, M., Coombs, D., Baly, D., Kabbinnavar, F. & Slamon, D. (1999). Inhibitory effects of combinations of HER-2/neu antibody and chemotherapeutic agents used for treatment of human breast cancers. *Oncogene* Vol. 18, No. 13, (Apr 1, 1999), pp. 2241-2251
- Pei, X. Y., Dai, Y. & Grant, S. (2004). Synergistic induction of oxidative injury and apoptosis in human multiple myeloma cells by the proteasome inhibitor bortezomib and histone deacetylase inhibitors. *Clin Cancer Res* Vol. 10, No. 11, (Jun 1, 2004), pp. 3839-3852
- Perez-Galan, P., Roue, G., Lopez-Guerra, M., Nguyen, M., Villamor, N., Montserrat, E., Shore, G. C., Campo, E. & Colomer, D. (2008). BCL-2 phosphorylation modulates sensitivity to the BH3 mimetic GX15-070 (Obatoclax) and reduces its synergistic interaction with bortezomib in chronic lymphocytic leukemia cells. *Leukemia* Vol. 22, No. 9, (Sep, 2008), pp. 1712-1720
- Pheng, S., Chakrabarti, S. & Lamontagne, L. (2000). Dose-dependent apoptosis induced by low concentrations of methylmercury in murine splenic Fas⁺ T cell subsets. *Toxicology* Vol. 149, No. 2-3, (Aug 21, 2000), pp. 115-128
- Platini, F., Perez-Tomas, R., Ambrosio, S. & Tessitore, L. (2010). Understanding autophagy in cell death control. *Curr Pharm Des* Vol. 16, No. 1, (Jan, 2010), pp. 101-113
- Poole, C. A., Brookes, N. H., Gilbert, R. T., Beaumont, B. W., Crowther, A., Scott, L. & Merrilees, M. J. (1996). Detection of viable and non-viable cells in connective tissue explants using the fixable fluorophores 5-chloromethylfluorescein diacetate and ethidium homodimer-1. *Connect Tissue Res* Vol. 33, No. 4, (1996), pp. 233-241

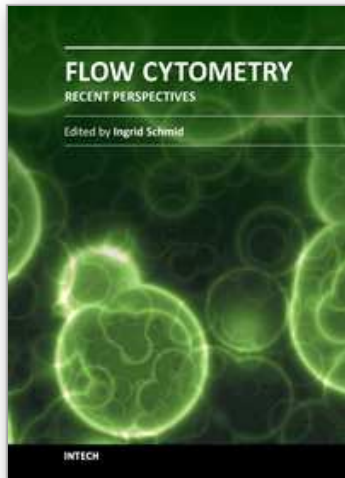
- Poot, M., Gibson, L. L. & Singer, V. L. (1997). Detection of apoptosis in live cells by MitoTracker red CMXRos and SYTO dye flow cytometry. *Cytometry* Vol. 27, No. 4, (Apr 1, 1997), pp. 358-364
- Prosperi, E., Croce, A. C., Bottiroli, G. & Supino, R. (1986). Flow cytometric analysis of membrane permeability properties influencing intracellular accumulation and efflux of fluorescein. *Cytometry* Vol. 7, No. 1, (Jan, 1986), pp. 70-75
- Prowse, A. B., Wilson, J., Osborne, G. W., Gray, P. P. & Wolvetang, E. J. (2009). Multiplexed staining of live human embryonic stem cells for flow cytometric analysis of pluripotency markers. *Stem Cells Dev* Vol. 18, No. 8, (Oct, 2009), pp. 1135-1140
- Radcliff, G., Waite, R., LeFevre, J., Poulik, M. D. & Callewaert, D. M. (1991). Quantification of effector/target conjugation involving natural killer (NK) or lymphokine activated killer (LAK) cells by two-color flow cytometry. *J Immunol Methods* Vol. 139, No. 2, (Jun 3, 1991), pp. 281-292
- Ramachandran, C., Resek, A. P., Escalon, E., Aviram, A. & Melnick, S. J. (2010). Potentiation of gemcitabine by Turmeric Force in pancreatic cancer cell lines. *Oncol Rep* Vol. 23, No. 6, (Jun, 2010), pp. 1529-1535
- Ross, D. D., Joneckis, C. C., Ordonez, J. V., Sisk, A. M., Wu, R. K., Hamburger, A. W. N. R. E. & Nora, R. E. (1989). Estimation of cell survival by flow cytometric quantification of fluorescein diacetate/propidium iodide viable cell number. *Cancer Res* Vol. 49, No. 14, (Jul 15, 1989), pp. 3776-3782
- Sarkar, A., Mandal, G., Singh, N., Sundar, S. & Chatterjee, M. (2009). Flow cytometric determination of intracellular non-protein thiols in *Leishmania* promastigotes using 5-chloromethyl fluorescein diacetate. *Exp Parasitol* Vol. 122, No. 4, (Aug, 2009), pp. 299-305
- Sebastia, J., Cristofol, R., Martin, M., Rodriguez-Farre, E. & Sanfeliu, C. (2003). Evaluation of fluorescent dyes for measuring intracellular glutathione content in primary cultures of human neurons and neuroblastoma SH-SY5Y. *Cytometry A* Vol. 51, No. 1, (Jan, 2003), pp. 16-25
- Shapiro, H. M. (2003). *Practical flow cytometry*. 4th Edition. Wiley-Liss. ISBN (9780471411253-0471411256) Hoboken, N.J.
- Shuck, S. C. & Turchi, J. J. (2010). Targeted inhibition of Replication Protein A reveals cytotoxic activity, synergy with chemotherapeutic DNA-damaging agents, and insight into cellular function. *Cancer Res* Vol. 70, No. 8, (Apr 15, 2010), pp. 3189-3198
- Sims, J. T. & Plattner, R. (2009). MTT assays cannot be utilized to study the effects of STI571/Gleevec on the viability of solid tumor cell lines. *Cancer Chemother Pharmacol* Vol. 64, No. 3, (Aug, 2009), pp. 629-633
- Sugiyama, K., Shimizu, M., Akiyama, T., Ishida, H., Okabe, M., Tamaoki, T. & Akinaga, S. (1998). Combined effect of navelbine with medroxyprogesterone acetate against human breast carcinoma MCF-7 cells in vitro. *Br J Cancer* Vol. 77, No. 11, (Jun, 1998), pp. 1737-1743
- Talbot, J. D., Barrett, J. N., Barrett, E. F. & David, G. (2008). Rapid, stimulation-induced reduction of C12-resorufin in motor nerve terminals: linkage to mitochondrial metabolism. *J Neurochem* Vol. 105, No. 3, (May, 2008), pp. 807-819

- Trudel, S., Li, Z. H., Rauw, J., Tiedemann, R. E., Wen, X. Y. & Stewart, A. K. (2007). Preclinical studies of the pan-Bcl inhibitor obatoclax (GX015-070) in multiple myeloma. *Blood* Vol. 109, No. 12, (Jun 15, 2007), pp. 5430-5438
- Ullal, A. J., Pisetsky, D. S. & Reich, C. F., 3rd. (2010). Use of SYTO 13, a fluorescent dye binding nucleic acids, for the detection of microparticles in in vitro systems. *Cytometry A* Vol. 77, No. 3, (Mar, 2010), pp. 294-301
- Vega, M. I., Martinez-Paniagua, M., Huerta-Yepez, S., Gonzalez-Bonilla, C., Uematsu, N. & Bonavida, B. (2009). Dysregulation of the cell survival/anti-apoptotic NF-kappaB pathway by the novel humanized BM-ca anti-CD20 mAb: implication in chemosensitization. *Int J Oncol* Vol. 35, No. 6, (Dec, 2009), pp. 1289-1296
- Wesierska-Gadek, J., Gueorguieva, M., Ranftler, C. & Zerza-Schnitzhofer, G. (2005). A new multiplex assay allowing simultaneous detection of the inhibition of cell proliferation and induction of cell death. *J Cell Biochem* Vol. 96, No. 1, (Sep 1, 2005), pp. 1-7
- West, C. A., He, C., Su, M., Swanson, S. J. & Mentzer, S. J. (2001). Aldehyde fixation of thiol-reactive fluorescent cytoplasmic probes for tracking cell migration. *J Histochem Cytochem* Vol. 49, No. 4, (Apr, 2001), pp. 511-518
- Wlodkowic, D. & Skommer, J. (2007). SYTO probes: markers of apoptotic cell demise. *Curr Protoc Cytom* Vol. Chapter 7, No., (Oct, 2007), pp. Unit7 33
- Woodcock, J., Griffin, J. P. & Behrman, R. E. (2011). Development of novel combination therapies. *N Engl J Med* Vol. 364, No. 11, (Mar 17, 2011), pp. 985-987
- Workman, P., Burrows, F., Neckers, L. & Rosen, N. (2007). Drugging the cancer chaperone HSP90: combinatorial therapeutic exploitation of oncogene addiction and tumor stress. *Ann N Y Acad Sci* Vol. 1113, No., (Oct, 2007), pp. 202-216
- Wright, J. J. (2010). Combination therapy of bortezomib with novel targeted agents: an emerging treatment strategy. *Clin Cancer Res* Vol. 16, No. 16, (Aug 15, 2010), pp. 4094-4104
- Yan, X., Habbersett, R. C., Yoshida, T. M., Nolan, J. P., Jett, J. H. & Marrone, B. L. (2005). Probing the kinetics of SYTOX Orange stain binding to double-stranded DNA with implications for DNA analysis. *Anal Chem* Vol. 77, No. 11, (Jun 1, 2005), pp. 3554-3562
- Yanamandra, N., Colaco, N. M., Parquet, N. A., Buzzeo, R. W., Boulware, D., Wright, G., Perez, L. E., Dalton, W. S. & Beaupre, D. M. (2006). Tipifarnib and bortezomib are synergistic and overcome cell adhesion-mediated drug resistance in multiple myeloma and acute myeloid leukemia. *Clin Cancer Res* Vol. 12, No. 2, (Jan 15, 2006), pp. 591-599
- Yeh, C. J., Hsi, B. L. & Faulk, W. P. (1981). Propidium iodide as a nuclear marker in immunofluorescence. II. Use with cellular identification and viability studies. *J Immunol Methods* Vol. 43, No. 3, (1981), pp. 269-275
- Zahorowska, B., Crowe, P. J. & Yang, J. L. (2009). Combined therapies for cancer: a review of EGFR-targeted monotherapy and combination treatment with other drugs. *J Cancer Res Clin Oncol* Vol. 135, No. 9, (Sep, 2009), pp. 1137-1148
- Zamai, L., Canonico, B., Luchetti, F., Ferri, P., Melloni, E., Guidotti, L., Cappellini, A., Cutroneo, G., Vitale, M. & Papa, S. (2001). Supravital exposure to propidium iodide identifies apoptosis on adherent cells. *Cytometry* Vol. 44, No. 1, (May 1, 2001), pp. 57-64

- Zanetti, M., d'Uscio, L. V., Peterson, T. E., Katusic, Z. S. & O'Brien, T. (2005). Analysis of superoxide anion production in tissue. *Methods Mol Med* Vol. 108, No., 2005), pp. 65-72
- Zhang, N., Wu, Z. M., McGowan, E., Shi, J., Hong, Z. B., Ding, C. W., Xia, P. & Di, W. (2009). Arsenic trioxide and cisplatin synergism increase cytotoxicity in human ovarian cancer cells: therapeutic potential for ovarian cancer. *Cancer Sci* Vol. 100, No. 12, (Dec, 2009), pp. 2459-2464

IntechOpen

IntechOpen



Flow Cytometry - Recent Perspectives

Edited by M.Sc. Ingrid Schmid

ISBN 978-953-51-0626-5

Hard cover, 500 pages

Publisher InTech

Published online 13, June, 2012

Published in print edition June, 2012

"Flow Cytometry - Recent Perspectives" is a compendium of comprehensive reviews and original scientific papers. The contents illustrate the constantly evolving application of flow cytometry to a multitude of scientific fields and technologies as well as its broad use as demonstrated by the international composition of the contributing author group. The book focuses on the utilization of the technology in basic sciences and covers such diverse areas as marine and plant biology, microbiology, immunology, and biotechnology. It is hoped that it will give novices a valuable introduction to the field, but will also provide experienced flow cytometrists with novel insights and a better understanding of the subject.

How to reference

In order to correctly reference this scholarly work, feel free to copy and paste the following:

Tomas Lombardo, Laura Anaya, Laura Kornbliht and Guillermo Blanco (2012). Median Effect Dose and Combination Index Analysis of Cytotoxic Drugs Using Flow Cytometry, *Flow Cytometry - Recent Perspectives*, M.Sc. Ingrid Schmid (Ed.), ISBN: 978-953-51-0626-5, InTech, Available from:

<http://www.intechopen.com/books/flow-cytometry-recent-perspectives/median-effect-dose-and-combination-index-analysis-of-cytotoxic-drugs-using-flow-cytometry>

INTECH
open science | open minds

InTech Europe

University Campus STeP Ri
Slavka Krautzeka 83/A
51000 Rijeka, Croatia
Phone: +385 (51) 770 447
Fax: +385 (51) 686 166
www.intechopen.com

InTech China

Unit 405, Office Block, Hotel Equatorial Shanghai
No.65, Yan An Road (West), Shanghai, 200040, China
中国上海市延安西路65号上海国际贵都大饭店办公楼405单元
Phone: +86-21-62489820
Fax: +86-21-62489821

© 2012 The Author(s). Licensee IntechOpen. This is an open access article distributed under the terms of the [Creative Commons Attribution 3.0 License](#), which permits unrestricted use, distribution, and reproduction in any medium, provided the original work is properly cited.

IntechOpen

IntechOpen